Viscous energy transfer in the boundary layer of the vortex tube

André Kaufmann *

23.03.2021

The vortex tube can separate a mass flow into a hot and cold mass flow. In this paper, the energy balance in the boundary layer of the vortex tube is analyzed with respect to a possible effect of temperature separation in the boundary layer by the viscous term of the enthalpy balance equation. A Large Eddy Simulation is used to generate the velocity profiles used for the computation of the viscous source terms. The dominant contributions of the source terms in the boundary layer of the vortex tube are identified and computed from the velocity fields. It is demonstrated how the strong velocity gradients in the boundary layer create a viscous flux of energy. An implementation of balance equations both with and without source term show the effect of energy separation in the boundary layer of the vortex tube.

1 Introduction

The vortex tube has attracted the interest of many scientists and engineers throughout the past. Numerous publications on experiments and CFD simulations have been issued since the discovery of temperature separation by Ranque [1] almost a century ago. The vortex tube has found several applications from the cooling of tools to the ventilation of clothing for firefighters. The experimental and numerical findings have been summarized in several review papers, see for instance Devade [2], Subudhi [3], Eiamsaard [4] and others.
In this paper the viscous terms in the energy balance equations are examined more closely with respect to a possible energy transfer in the boundary layer resulting in a temperature difference. Moreover velocity profiles resulting from a Large Eddy Simulation (LES) of the vortex tube are used to examine the source terms in the enthalpy

*Ravensburg-Weingarten UAS Andre.Kaufmann@rwu.de

balance equation. Solutions of the sensible enthalpy balance equations with the correctly implemented viscous source term in a CFD code are used to investigate the resulting enthalpy distribution in the boundary layer. A comparison with a balance equation ignoring the corresponding viscous source term demonstrates the effect of the viscous terms on temperature separation in the vortex tube. Throughout the paper the notation for vectors and tensors of Altenbach [5] is used. All balance equations are taken from Aris [6] and other reference works on fluid dynamics, for instance Candel [7].

2 Temperature separation in the vortex tube

Before CFD was widely accessible, investigations on the vortex tube were performed by experiment. In most cases, measurement was limited to mass flow fraction, expansion ratio and temperature at the inlet and the outlets. This only allowed to verify the global balances on the vortex tube. The corresponding results are briefly repeated as they serve as a basis for further detailed discussions.

2.1 Mass and energy conservation

By thermodynamic convention the mass flow entering the vortex tube $\dot{m}_i$ is positive and the cold mass flow $\dot{m}_c$ and hot mass flow $\dot{m}_h$ leaving the vortex tube are negative. By conservation of mass, the mass flow must sum up to zero.

$$\dot{m}_i + \dot{m}_c + \dot{m}_h = 0 \tag{1}$$

An important parameter in the temperature splitting was found to be the fraction of mass flow leaving the cold side of tube $\dot{m}_c/\dot{m}_i$ compared to the total mass flow entering the tube.

$$\mu = \frac{|\dot{m}_c|}{\dot{m}_i} \tag{2}$$

The temperature separation reaches its maximum in most experiments and applications at a mass flow ratio of $\mu \approx 0.3$. Experiments then show a strong separation of temperature depending on the expansion ratio in the tube. The enthalpy fluxes at inlet and outlets can be used in a corresponding balance equation. By thermodynamic convention, the enthalpy flux entering the tube $\dot{H}_i$ is positive and the enthalpy fluxes leaving the tube $\dot{H}_c$ and $\dot{H}_h$ are negative. Energy conservation requires the enthalpy fluxes to add up to zero.

$$\dot{H}_i + \dot{H}_c + \dot{H}_h = 0 \tag{3}$$

The fluid is assumed to have the characteristics of a calorically perfect gas $\dot{H} = \dot{m} c_p T$. This yields a direct link from the enthalpy h_s to the temperatures T by $h = c_p T$. The maximum enthalpy flux separation is achieved in most experiments at a mass flow ratio of $\mu \approx 0.6$. Since the vortex tube does not contain any moving parts, the flow structure itself must be at the origin of the enthalpy transfer.

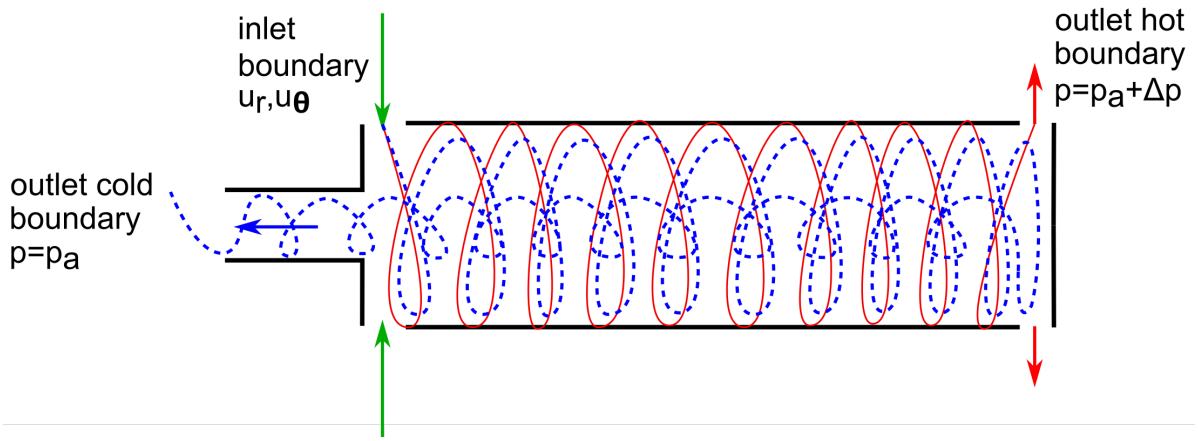

Figure 1: Sketch of the cross section of the vortex tube.

3 Flow structure in the vortex tube

Many CFD simulations have been carried out to determine the flow structure in the vortex tube and are accessible in the literature, see for instance the review of Eiamsaard [4]. Well documented are the results of Farouk et al. [8],[9]. They include velocity profiles and temperature fields. This computational geometry is chosen, so comparison with existing results can be done. The computational geometry of Farouk et al. [8] consists of a cylinder with a diameter of $d = 20\,mm$ and a length of $l = 100\,mm$. The inlet consists of the first part of the cylinder with a length of $3\,mm$, the hot outlet is placed at the end of the tube with a length of $1.5\,mm$. The cold outlet is added in form of a smaller cylinder at the center of the tube on the inlet side.

3.1 Typical Reynolds numbers

The Reynolds number in the vortex tube is estimated using a characteristic velocity of $u_0 = 200\,m/s$, the tube diameter $d = 0.02\,m$ an the ambient viscosity of air $\nu = 1.5e-5\,m^2/s$.

$$Re_d = \frac{u_0\, d}{\nu} = 2.67 \cdot 10^5 \tag{4}$$

Based on the Reynolds number, the flow is thus expected to show a fully developed turbulent character. For the boundary layer, a representative length of half of the tube length, $x = 50\,mm$ is chosen. Using the standard approximation, see Schlichting [10], this leads to the thickness δ.

$$\delta \approx 0,37 \frac{x}{Re_d^{1/5}} = 1.52 \cdot 10^{-3} m \tag{5}$$

The boundary layers are expected to take less than one-tenth of the tube diameter and the numerical computation requires a corresponding grid resolution in the boundary layer.

3.2 Estimation of grid properties

A Large Eddy Simulation (LES) requires $y+ = 1$ for the boundary grid spacing. The corresponding grid spacing Δs is computed using the friction coefficient proposed by Schlichting.

$$\begin{aligned} C_f &= (2\log_{10}(Re_d) - 0.65)^{-2.3} = 4.79 \cdot 10^{-3} \\ \frac{\tau_w}{\rho} &= C_F \frac{1}{2} u_{max}^2 = 95,7\, m^2/s^2 \\ u^* &= \sqrt{\frac{\tau_w}{\rho}} = \sqrt{C_F \frac{1}{2} u_{max}^2} = 9,78\, m/s \\ \Delta s &= y^+ \frac{\nu}{u^*} = 1.53 \cdot 10^{-6}\, m \end{aligned}$$

A uniform grid spacing based on the boundary layer grid spacing $1.5 \cdot 10^{-6}\, m$ leads to a prohibitive grid size and computational effort. Therefore, the grid is refined from the center to the boundary layer, preserving a reasonable grid spacing in the center of the tube.

3.3 Choice of numerical solver

Burazer et al. [11] report the use of different *OpenFoam* solvers and present solutions of the velocity profiles in the vortex tube. Compressibility effects are not expected to alter the flow structure significantly in the boundary layer. Therefore the computation is carried out with an incompressible solver. For the results presented, the *pisoFoam* solver from the *OpenFoam* package is chosen. *pisoFoam* solves the incompressible Navier-Stokes equations and allows the use of different turbulence models. The dynamic k-equation model is used for the computation of turbulent viscosity in the Large Eddy Simulation (LES).

3.4 Boundary conditions

The boundary conditions for the LES are chosen to be representative for the flow in the vortex tube. At the inlet a circumferential velocity of $u_{\theta,0} = 300\, m/s$ is imposed simultaneously with a radial inflow velocity of $u_r = -10\, m/s$. At the hot orifice the ambient pressure of $p = 1\, bar$ is imposed. At the cold outlet in the center of the tube, a volumetric flow rate corresponding to 1/3 of the inlet flow rate is imposed.
This combination of boundary conditions guarantees to deliver a stable simulation.

3.5 Characteristic time scale

For the estimation of the necessary physical simulation time the characteristic time scale is estimated by the volumetric inlet flow rate $\dot{V}_{in}$ and the volume of the vortex tube V_{tube}.

$$\tau_c = \frac{V_{tube}}{\dot{V}_{in}} \tag{6}$$

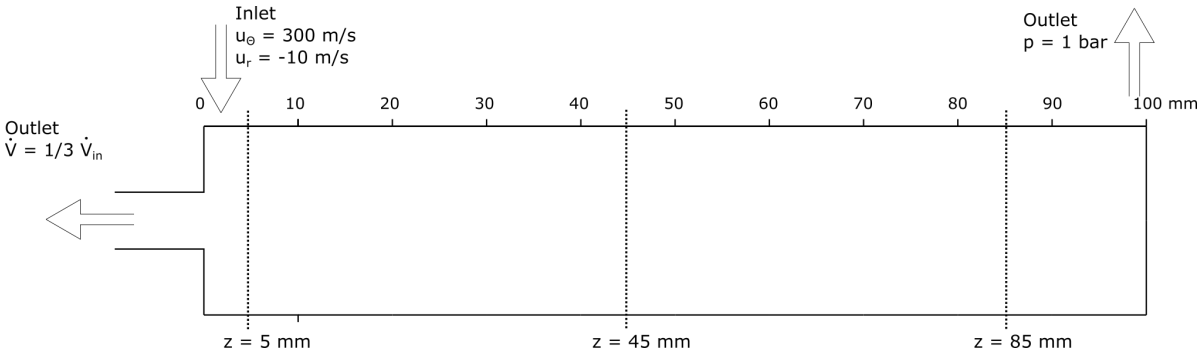

Figure 2: Sketch of the vortex tube with profile sections at z=5 mm, z= 45 mm and z=85 mm

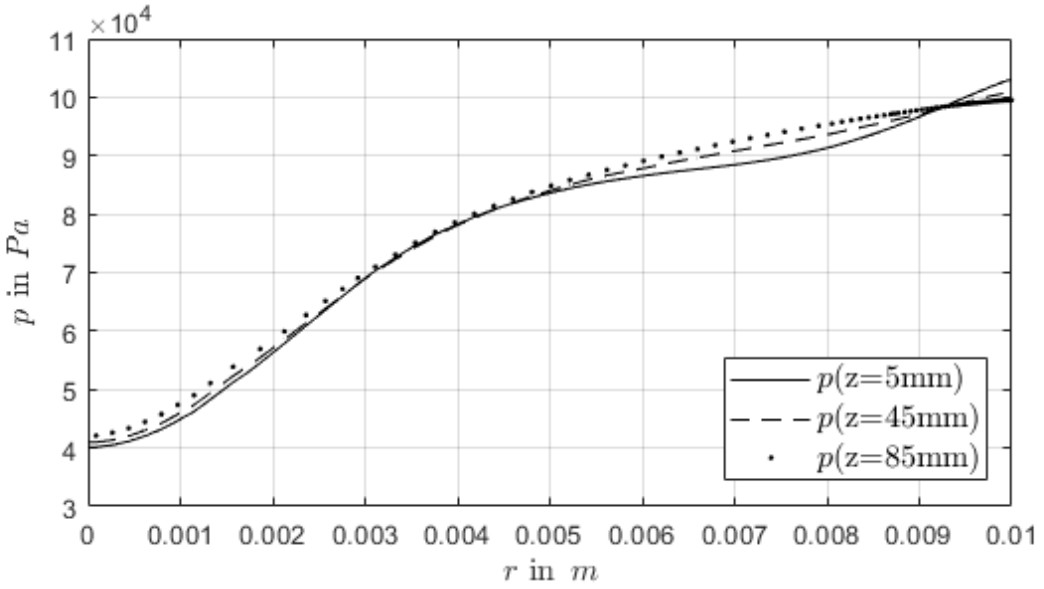

Figure 3: Time averaged profiles of pressure in the vortex tube

Since the boundary at the cold central exit is set to 1/3 of the inlet mass flow rate, the volume can be expected to be completely flushed by the inlet condition after roughly 3 τ_c. This condition is monitored by convecting a passive scalar. Time-averaging is started after 10 characteristic time scales.

3.6 Axial and circumferential velocity profiles

In fig.2 three sections are marked. At those cut sections time-averaged pressure p, axial velocity u_z and tangential velocity u_θ are extracted from the LES solution along the section. The pressure profiles from the sections are shown in fig. 3. Due to the high swirling velocity, there is a significant pressure difference between the tube wall and the center of the tube.

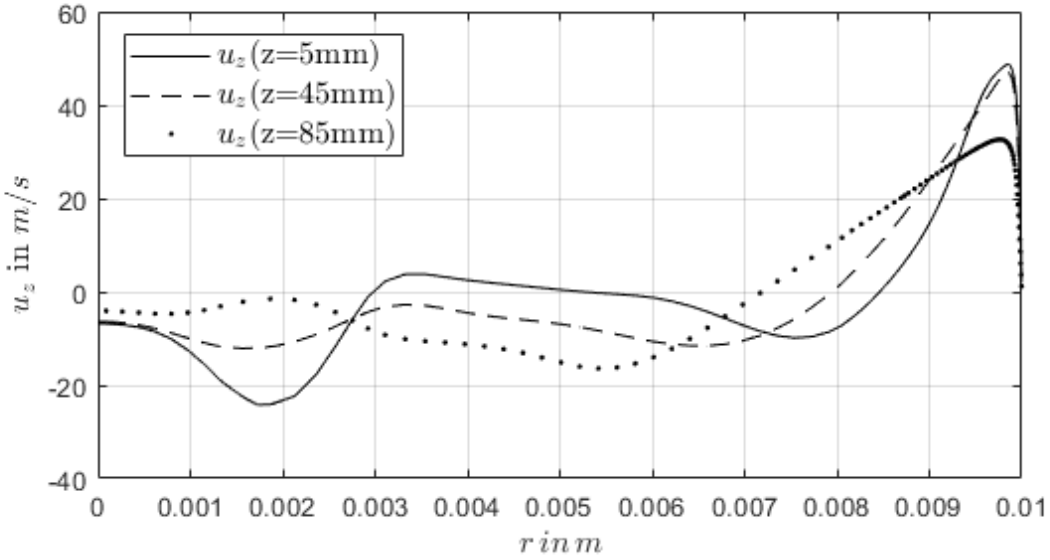

Figure 4: Time-averaged profiles of axial velocity in the vortex tube

Axial velocity profiles at the different cut sections are shown in fig. 4. The highest axial velocities occur next to the tube wall and cause strong gradients in u_z.

In figure 4 the instantaneous axial velocity profile is shown at different sections after approx 15 characteristic time scales.

4 Enthalpy balance

The influence of the boundary layer on the effect of temperature separation is studied following the total specific enthalpy h_t balance. The total enthalpy h_t comprises the sensible enthalpy h_s and the kinetic energy $1/2\,\vec{u}.\vec{u}$.

$$h_t = h_s + \frac{1}{2}\vec{u}.\vec{u} \tag{7}$$

In the first step, the corresponding balance equations are analyzed.

4.1 Enthalpy balance equations

The balance of total specific enthalpy shows, next to the transport and temporal change of pressure contributions due to the diffusion of temperature, a source term due to viscous effects.

$$\frac{\partial}{\partial t}\rho h_t + \nabla.\left(\rho h_t \vec{u}\right) = \frac{\partial}{\partial t}p + \nabla.\left(\lambda \nabla T\right) + \nabla.\left(\bar{\tau}.\vec{u}\right) \tag{8}$$

The diffusive heat flux $\dot{\vec{q}}$ is present whenever temperature gradients are present in the flow.

$$\dot{\vec{q}} = -\lambda \nabla T \tag{9}$$

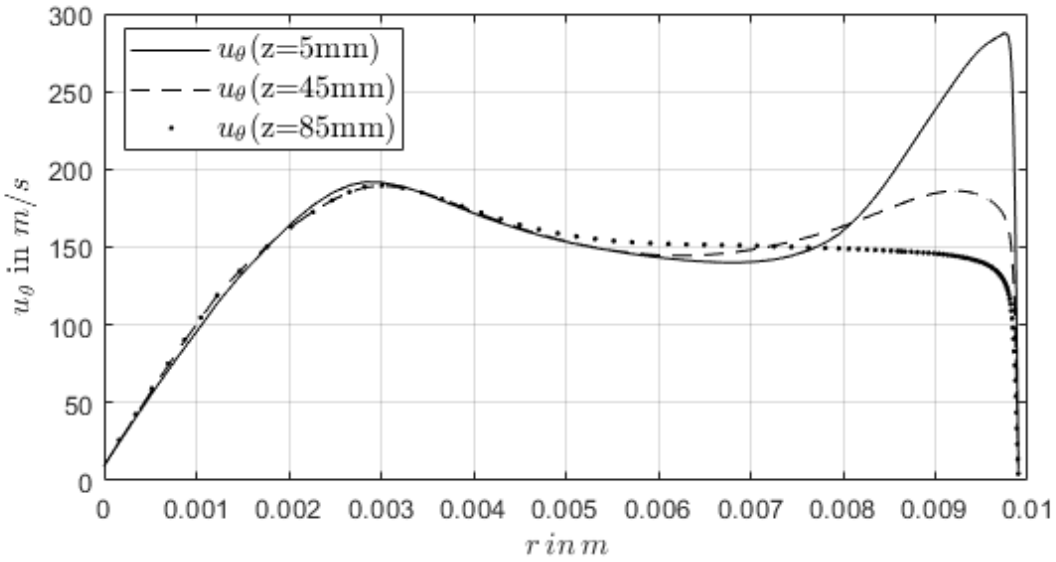

Figure 5: Time-averaged profiles of circumferential velocity in the vortex tube

Imposing the adiabatic condition with $\nabla T = 0$ at the boundaries, the integral over the computational domain vanishes.

$$\int_V \nabla.\left(\lambda \nabla T\right) dV = \int_A \left(\lambda \nabla T\right) .\vec{n} dA = 0 \tag{10}$$

Therefore, the diffusive heat flux does not contribute to the global total enthalpy change if the tube is isolated and an adiabatic condition can be assumed.

In the viscous term, $\bar{\tau} = \mu((\nabla \vec{u}) + (\nabla \vec{u})^T - \frac{2}{3}\mathbb{1}(\nabla.\vec{u}))$ is the stress tensor. The viscous term is often omitted in the enthalpy equation since it does not deliver a significant contribution in most flows. However, Burazer et al. [11] have reported that the temperature separation can only be reproduced through CFD codes with a correct implementation of the viscous term.
The viscous term exhibits a viscous energy flux $\vec{e_\nu}$.

$$\vec{e_\nu} = -\bar{\tau}.\vec{u} \tag{11}$$

This flux contribution is small in normal conditions whereas the diffusive flux due to temperature gradients is usually much larger.
The viscous contribution can be integrated over the computational domain to compute the expected change in the total enthalpy balance.

$$\int_V \nabla.\left(\bar{\tau}.\vec{u}\right) dV = \int_A \left(\bar{\tau}.\vec{u}\right) .\vec{n} dA \tag{12}$$

On the tube walls, the velocity is zero due to the no-slip condition. Therefore there is no energy flux across the walls due to the viscous contribution. Except for the inlet

and outlet boundaries, the viscous term does not alter the total enthalpy balance in the vortex tube.

If the total enthalpy balance (eq. 8) is integrated over the total domain, the global enthalpy balance (eq. 3) is recovered. Studying the effects of the total enthalpy balance should therefore lead to some information concerning the temperature separation.

4.2 Dominant effects in enthalpy balance

A simple method to determine dominant effects in the balance equations is dimensional analysis. For the sake of simplification, thermal conductivity λ, viscosity ν and specific heat capacity c_p have beem kept constant in this analysis. The total enthalpy balance equation has been made non-dimensional by the introduction of reference values for length l_0, velocity u_0, temperature T_0 and density ρ_0. Characteristic time scales have been obtained by the combination of velocity and length scale l_0/u_0 and the characteristic dynamic viscosity from density and viscosity $\mu_0 = \rho_0\nu$. The ratio of heat capacities thus is noted by $\kappa = c_p/c_v$. Non-dimensional quantities are marked with a star $*$.

$$\begin{aligned}\frac{\partial}{\partial t^*}\rho^* h_t^* + \nabla^*.(\rho^* h_t^* \vec{u}^*) =& \frac{\kappa-1}{\kappa}\frac{\partial}{\partial t^*}p^* \\ &+ Fo\nabla^*.(\lambda\nabla T^*) \\ &+ \frac{Ec}{Re}\nabla^*.(\bar{\tau}^*.\vec{u}^*)\end{aligned} \tag{13}$$

The diffusive heat flux contribution is preceded by the Fourier number Fo. The Fourier number compares the time scales of temperature diffusion to the time scale of convection.

$$Fo = \frac{\lambda}{\rho_0 c_p l_0 u_0} \tag{14}$$

The viscous term is preceeded by the ratio of Eckert to Reynolds number. The Eckert number Ec compares the kinetic energy to the enthalpy.

$$Ec = \frac{u_0^2}{c_p T_0} \tag{15}$$

The effects of heat transfer by diffusion can be compared to the viscous effects by taking the ratio of the factors preceding the terms in the non-dimensional equation.

$$\frac{Fo \cdot Re}{Ec} = \frac{\lambda}{\rho_0 c_p l_0 u_0} \cdot \frac{\rho_0 c_p T_0 l_0}{\mu_0 u_0} = \frac{\lambda T_0}{\mu_0 u_0^2} \tag{16}$$

When this ratio is clearly larger unity, the diffusive effects due to temperature diffusion are larger than the contribution of the viscous effects that may lead to a temperature separation by the viscous energy flux (eq. 11). This is best understood by an illustrative example: In the case of air at ambient conditions and moderate velocity ($u_0 = 5\,m/s$, $\lambda_0 = 0.025\,W/mK$, $\Delta\, T_0 = 10\,K$,$\mu = 2.5 \cdot 10^{-5}\,kg/ms$) the ratio is large $\frac{Fo \cdot Re}{Ec} = 400$ and

the effect of heat diffusion due to temperature difference dominates the redistribution of total enthalpy.
In the case of the vortex tube, however, the characteristic velocity is much larger. Taking $u_0 = 300m/s$ the ratio becomes $\frac{Fo \cdot Re}{Ec} = 0.11$. Here the viscous term dominates the right-hand side contribution of the total enthalpy balance. It can be concluded, that high velocities make the viscous term contribute significantly more to the right-hand side of the total enthalpy balance equation.

4.3 Total enthalpy source term in the vortex tube

The viscous source term Φ_{ht} in the total enthalpy balance contains the product of the stress tensor and the velocity gradient tensor.

$$\Phi_{ht} = \nabla . \left(\bar{\tau} . \vec{u} \right) \tag{17}$$

The stress tensor itself is constructed on the velocity gradient tensor. Therefore, this term can be expected to have significant impacts in the regions of strong velocity gradients. In the section on the velocity profiles of the vortex tube 3.6, it was illustrated that strong gradients occur in the boundary layer next to the tube wall. The dominant contributions with the highest tangential and axial velocities (u_θ, u_z) can be estimated by ignoring all other contributions but the radial dependence.

$$\begin{aligned} \Phi_{ht} \approx \mu \Bigg[& \left(\frac{u_z}{r} \frac{\partial}{\partial r} \left(r \frac{\partial}{\partial r} u_z \right) + \left(\frac{\partial}{\partial r} u_z \right)^2 \right) \\ & + \frac{1}{r} \frac{\partial}{\partial r} \left(r \left(\frac{\partial u_\theta}{\partial r} - \frac{u_\theta}{r} \right) u_\theta \right) \Bigg] \end{aligned} \tag{18}$$

Here, the source term Φ_{ht} is computed in postprocessing the velocity profiles in the three-dimensional grid as illustrated in fig. 6.

Since the dominant velocity gradients occur in the boundary layer due to the circumferential velocity u_θ and axial velocity u_z, the diagram shows only the boundary layer contributions. Due to the higher circumferential velocity u_θ magnitude the corresponding contribution is by one magnitude larger than the contribution due to the axial velocity u_z.
In this example, the source terms occur dominantly in a layer of 1/10 of a millimetre thickness. This is one order of magnitude smaller than the estimate for the boundary layer thickness following the estimation with the correlation by Schlichting. The source term is strongly positive directly on the tube wall and negative at a small distance from the tube wall. This behavior is analyzed more deeply by investigating the viscous energy flux: Ignoring all derivatives in the axial and circumferential direction, the viscous energy flux shows two remaining contributions in the radial direction.

$$\vec{e}_\nu = -\bar{\tau} . \vec{u} \approx \underbrace{-\mu u_\theta \left(\frac{\partial u_\theta}{\partial r} - \frac{u_\theta}{r} \right) \vec{n}_r}_{\vec{e}_{\nu,u_\theta}} \underbrace{-\mu u_z \left(\frac{\partial u_z}{\partial r} \right) \vec{n}_r}_{\vec{e}_{\nu,u_z}} \tag{19}$$

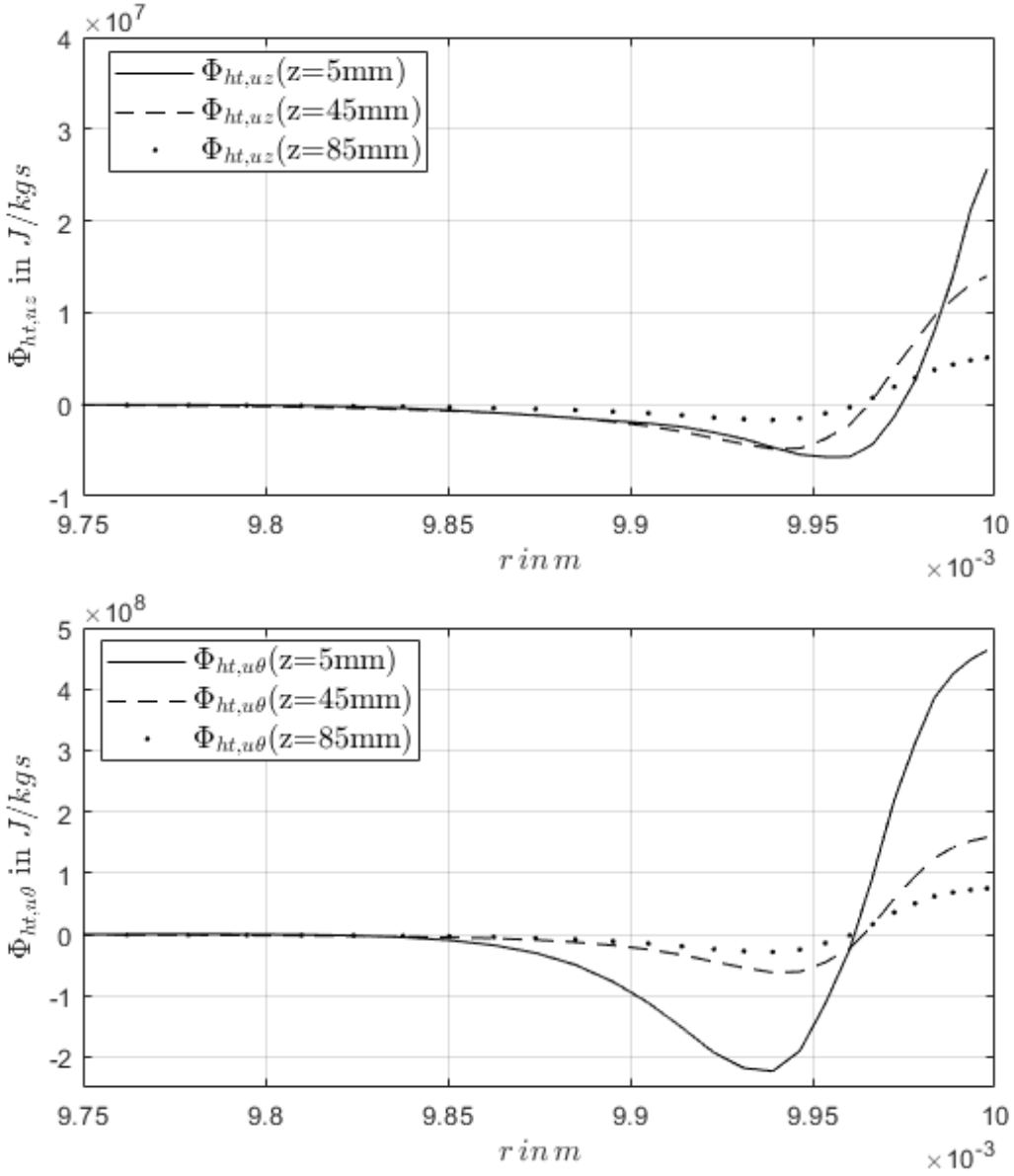

Figure 6: Total enthalpy source terms in the vortex tube at different sections, computed from time-averaged velocity profiles. Contributions of u_θ and u_z are shown separately.

The contribution associated with the circumferential velocity u_θ results from the difference of the velocity profile to a solid body rotation. Near the tube wall with a no-slip velocity boundary condition, the overall contribution of the derivative of the circumferential velocity u_θ is negative. Considering all signs, this creates a positive contribution to the flux in the positive radial direction. The resulting positive radial energy flux transports energy from the region of high circumferential velocity to the wall.

The contributions are computed directly by postprocessing the corresponding time-averaged velocity profiles. They are illustrated in fig. 7 for the boundary layer. Outside the boundary layer, the contributions are very small. In this case the radial energy flux $\vec{e}_\nu$ due to the circumferential velocity u_θ is much larger than the contribution due to the axial velocity u_z. This is due to the higher circumferential velocity magnitude.
The diagram shows that some energy is transferred by viscous effects from the region of high-velocity magnitude to the region closer to the wall and to a smaller extent from the region of high-velocity magnitude to the center of the wall. Since the energy flux is limited to the region of high-velocity gradients, the dominant energy flux is going on in a layer of 1/10 of a millimeter of the wall.

5 The energy transfer mechanism in detail

The energy transfer mechanism can be described in detail by considering the different energy balance equations. Additionally to the total enthalpy, the sensible enthalpy and the kinetic energy are discussed in detail to uncover the energy transfer mechanism.

5.1 Transport equations and source terms

Transport equations for the sensible enthalpy can be found in standard textbooks on fluid dynamics, see for instance Candel [7].

$$\frac{\partial}{\partial t}\rho h_s + \nabla.\,(\rho h_s \vec{u}) = \frac{d}{dt}p + \nabla.\,(\lambda \nabla T) + \bar{\tau}\colon\ (\nabla \vec{u}) \tag{20}$$

The viscous term $\bar{\tau}\colon\ (\nabla \vec{u})$ can take only positive values as kinetic energy is transferred by friction into enthalpy. Negative contributions would violate the second law of thermodynamics. When examining the contributions in detail, it is found that only squares of gradients occur and the contributions must therefore be positive.

Considering only the dominant contributions with derivatives in radial direction, the viscous source term takes a simple form in cylinder coordinates.

$$\begin{aligned} \Phi_{hs} &= \bar{\tau}\colon\ (\nabla \vec{u}) \\ &\approx \mu \left[\left(\frac{\partial u_\theta}{\partial r} - \frac{u_\theta}{r} \right)^2 + \left(\frac{\partial u_z}{\partial r} \right)^2 \right] \end{aligned} \tag{21}$$

The contribution from circumferential velocity u_θ and from velocity in the axial direction u_z, arise from the squares of the derivatives. Therefore, the contributions are always positive and are dominant in regions with strong derivatives.

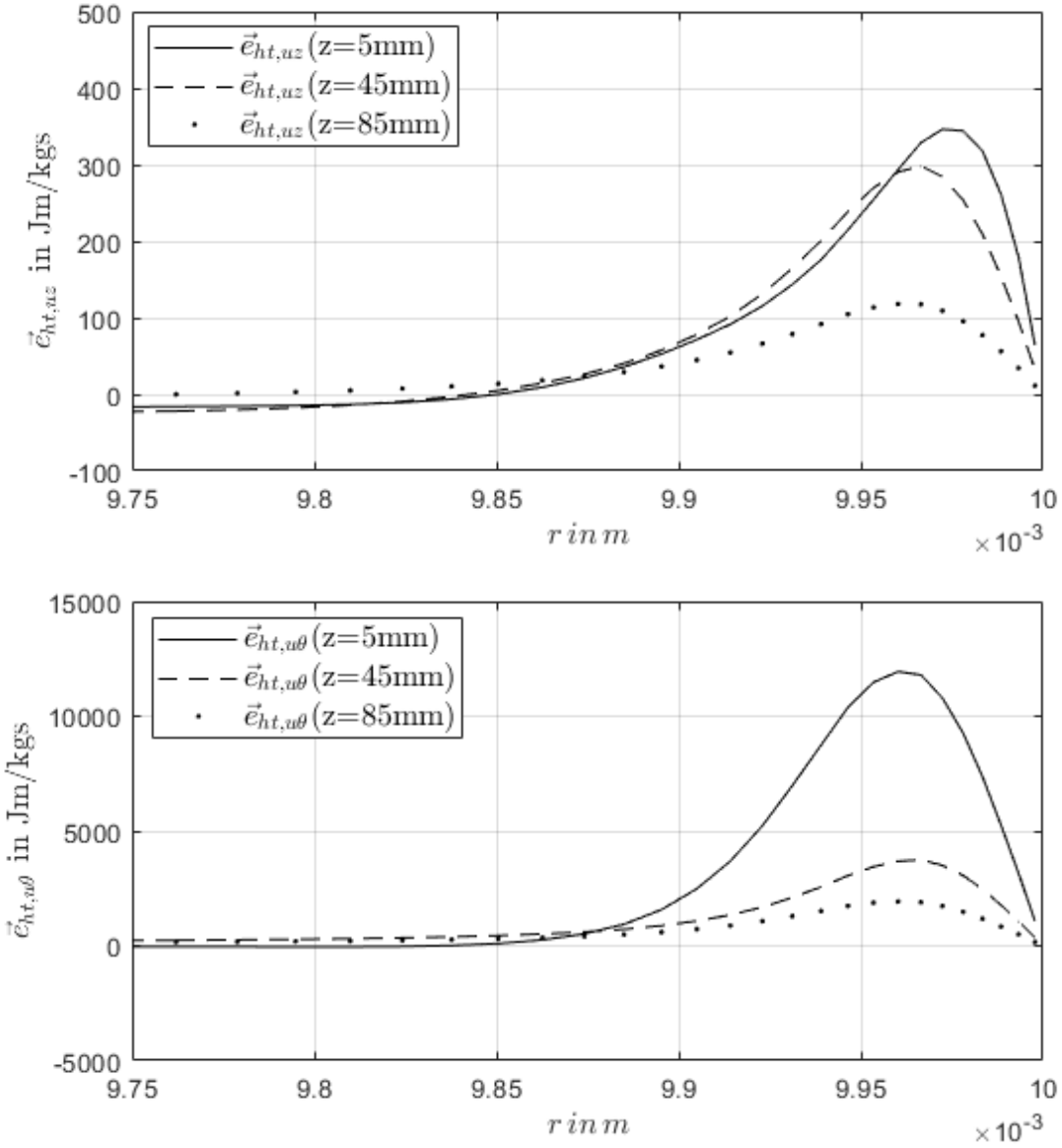

Figure 7: Viscous radial enthalpy flux in the vortex tube at different sections

The kinetic energy balance is obtained from the Navier-Stokes equations by taking the scalar product with the velocity $\vec{u}$.

$$\frac{\partial}{\partial t}\frac{1}{2}\rho\vec{u}.\vec{u} + \nabla.\left(\frac{1}{2}\rho\vec{u}.\vec{u}\vec{u}\right) = -\nabla p.\vec{u} + \left(\nabla.\bar{\tau}\right).\vec{u} \tag{22}$$

The viscous source term in the kinetic energy equation $\left(\nabla.\bar{\tau}\right).\vec{u}$ can take positive as well as negative values. It is expected that this term is dominantly negative in the boundary layer transferring kinetic energy by friction into sensible enthalpy.

The dominant contributions with derivatives in the radial direction are expressed in cylindrical coordinates.

$$\begin{aligned} \Phi_{Kin} &= \left(\nabla.\bar{\tau}\right).\vec{u} \\ &\approx \mu u_\theta\left[\frac{2}{r}\left(\frac{\partial u_\theta}{\partial r} - \frac{u_\theta}{r}\right) + \frac{\partial}{\partial r}\left(\frac{\partial u_\theta}{\partial r} - \frac{u_\theta}{r}\right)\right] \\ &\quad + \mu u_z\left[\frac{1}{r}\frac{\partial u_z}{\partial r} + \frac{\partial^2 u_z}{\partial r^2}\right] \end{aligned} \tag{23}$$

The contributions may be both, positive and negative. Next to the wall, the non-slip condition $\vec{u} = 0$ causes strong negative contributions of $\frac{\partial u_\theta}{\partial r}$ and $\frac{\partial u_z}{\partial r}$. They lead to negative contributions next to the wall. With velocity profiles different from the solid body rotation in the center of the tube, even positive contributions can occur.

5.2 Scale factor for the viscous contributions

All three source terms Φ_{ht}, Φ_{hs}, and Φ_{Kin} share the identical scaling factor $\mu\, u_0^2/l_0^2$.
The strong derivatives all occur in the boundary layer of the flow. Therefore a candidate for an appropriate length scale is the thickness of the boundary layer $l_0 = \delta$ estimated previously to dimension the grid spacing.
However, the velocity profiles resulting from the LES computation show a smaller distance from the maximum of the tangential velocity u_θ maximum to the wall than the estimated boundary layer thickness. Therefore, the adequate length scale is significantly smaller and a different length scale might be appropriate. A more sophisticated estimation for the thickness of the boundary layer in flow with very high rotational velocities may be helpfull in this respect.

5.3 Turbulent contribution to the source terms

In the previously shown figures, the source terms were computed from the time-averaged velocity profiles. This leads to smaller source terms than what would be expected from instantaneous velocity profiles since time-averaged velocity profiles have significantly smoother gradients. Further smoothing of gradients occurs due to the turbulent viscosity introduced by the turbulence model. Therefore, a quantitatively correct estimate of the source terms can only be given with the knowledge of the full knowledge of the velocity contributions and requires a true direct numerical simulation (DNS) of the flow.

6 Transport equations with and without source terms

The demonstrated effects of the source terms on the enthalpy equation are not sufficient to prove that the enthalpy separation is a result of the total enthalpy source term. A quantitative study is attempted by solving the sensible enthalpy equation with and without source terms in the CFD code.

6.1 Sensible enthalpy transport equations

For the illustration of the different right-hand side terms of the sensible enthalpy equation, two different transport equations are implemented into the CFD code:

- h_s is the transport of sensible enthalpy without the time derivative of pressure $\frac{\partial p}{\partial t}$.

$$\frac{\partial}{\partial t}\rho h_s + \nabla.\left(\rho h_s \vec{u}\right) = \nabla p.\vec{u} + \nabla.\left(\frac{\lambda}{c_p}\nabla h_{sn}\right) + \bar{\tau}:\ (\nabla\vec{u}) \tag{24}$$

- h_{sn} neglects the time derivative of pressure and the viscous term Φ_{hs}.

$$\frac{\partial}{\partial t}\rho h_{sn} + \nabla.\left(\rho h_{sn} \vec{u}\right) = \nabla p.\vec{u} + \nabla.\left(\frac{\lambda}{c_p}\nabla h_{sn}\right) \tag{25}$$

The time derivative of pressure $\frac{\partial p}{\partial t}$ is omitted from all equations to exclude effects resulting from pressure oscillations. Here, the sensible energy equation h_s is chosen for the transport equations, since the implementation of the viscous term $\nabla.(\bar{\tau}.\vec{u})$ delivering correct values is congruent with standard numerical schemes.

Before the transient simulation, the transport equations are initialized with a uniform field with the values $h_s = 300\,kJ/kg$ and $h_{sn} = 300\,kJ/kg$. The inlet boundary condition is set to $h_s = 255\,kJ/kg$. This corresponds to a total enthalpy of $h_t = h_s + \frac{1}{2}\vec{u}.\vec{u} = 275\,kJ/kg$. The transient simulation is carried out for approx. 10 convective times before the temporal averaging of h_s and h_{sn} is started. The field solutions are then time-averaged for approx 5 convective times.
Fig. 8 shows the time-averaged solutions for the transport equations h_s and h_{sn} in the previously defined tube cross sections. All in all the values for h_{sn} are roughly $20\,kJ/kg$ lower than h_s with identical boundary conditions. This shows the strong impact of the viscous term on the overall flow.
Towards the center of the tube, the values of both h_s and h_{sn} are significantly lower due to the term $\nabla p.\vec{u}$ showing another key working mechanism of the vortex tube.
The largest differences occur in the boundary layer of the flow. In the case of h_{sn} the values are slightly smaller than the inlet condition. Values of h_s in the boundary layer are significantly higher at some distance from the inlet. Approximate values for the total enthalpy h_t are computed by postprocessing the results of the enthalpy time-averaged transport equations h_s and h_{sn}, as well as the time averaged velocity fields by equation 7. This approach ignores the fluctuating components and therefore underestimates the total temperature. Still, it offers an idea of the development of the total temperature next to

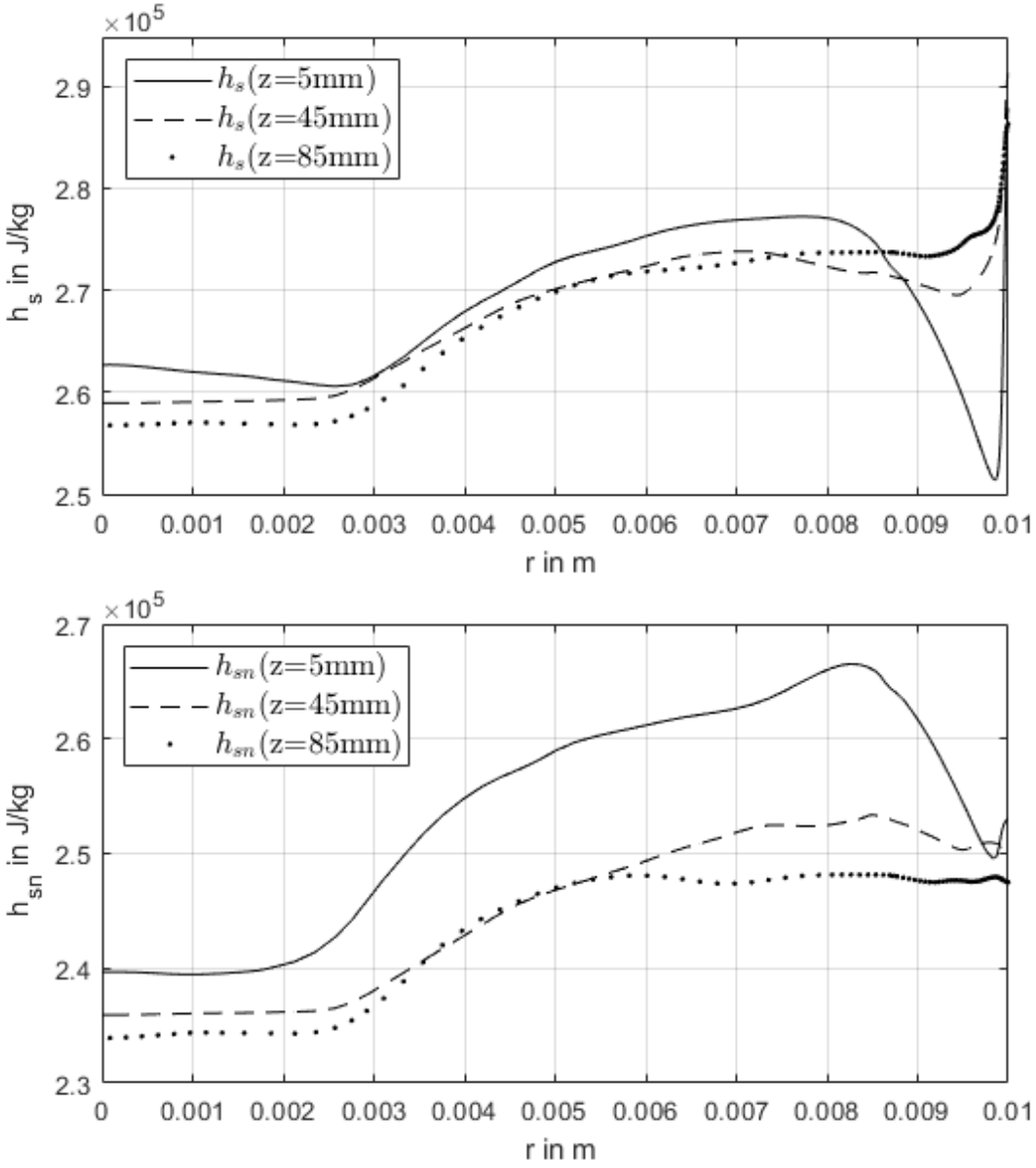

Figure 8: The time-averaged transport equations h_s and h_{sn} at the tube cross sections

the wall. Fig. 6.1 shows the values for h_t and h_{tn} in the boundary layer at the previously defined tube cross-sections. Neglecting the viscous term as in the case of h_{tn} the values for the total temperature in the boundary layer are roughly $30\,kJ/kg$ smaller next to the wall.
In the vortex tube, a significant amount of the flow leaving the tube at the hot orifice passes through this geometric region and is largely affected by the transport of kinetic energy towards the boundary layer.

7 Discussion and Conclusions

The implementation of the transport equations h_s and h_{sn} quantitatively confirms the work of Van Deemter [12]. The quantitative evaluation of the viscous contribution shows that it is a significant part of the energy transfer mechanism in the vortex tube. The energy transfer mechanics can not only be explained by the contribution of $\nabla p.\vec{u}$.
The viscous term in the total enthalpy equation h_t can be looked at as a flux contribution not only shifting kinetic energy to sensible enthalpy but also as the flux of energy in the boundary layer from the zones of high velocities to lower velocities.
The dimensional analysis reveals that this mechanism is covered in most types of flow by the thermal diffusion $\nabla.(\lambda\nabla T)$ and only in cases of very high-velocity gradients the viscous contribution may become the apparent dominant contribution.

Acknowledgements

This work was carried out during the research term granted by the RWU of applied sciences in spring 2020. All numerical simulations were performed on the RWU computational resources. No funding was received for conductiong this study.

Conflict of interest

The author has no conflicts of interest relevant to the content of this article. The *openFoam* software is available on the corresponding website.

References

[1] G. Ranque, Journal de Physique et Le Radium pp. 112–114 (1933)

[2] K.D. Devade, A. Pise, American Journal of Heat and Mass Transfer **4**, 115 (2017)

[3] S. Subudhi, M. Sen, Renewable and Sustainable Energy Reviews **52**, 172 (2015)

[4] S. Eiamsa-ard, P. Promvonge, Renewable and Sustainable Energy Reviews **12**(7), 1822 (2008)

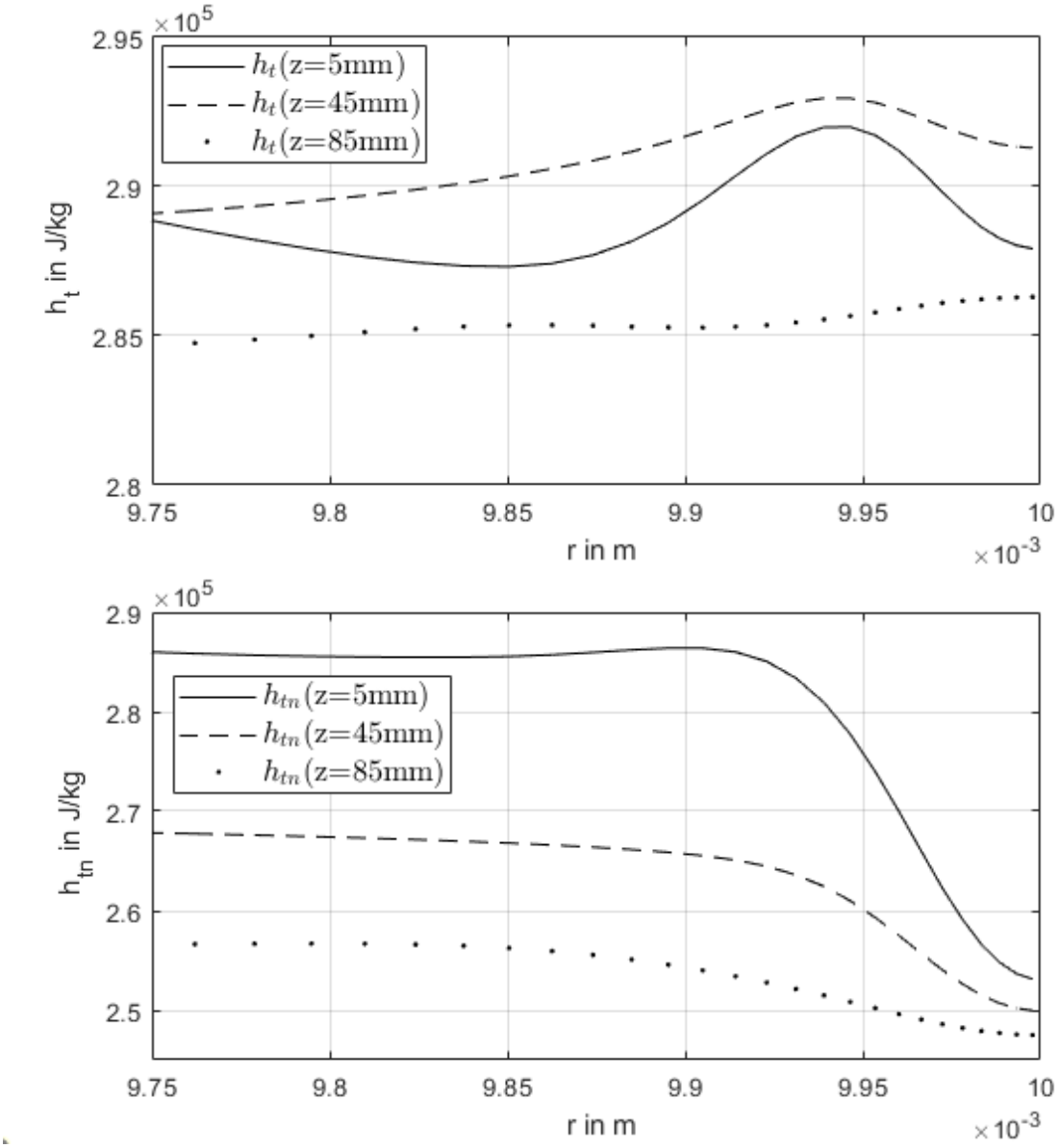

Figure 9: The time averaged transport equations h_t and h_{tn} in the boundary layer of the tube

[5] H. Altenbach, *Kontinuumsmechanik* (Springer, 2015)

[6] R. Aris, *Vectors, Tensors and the Basic Equations of Fluid Mechanics* (Dover, 1962)

[7] S. Candel, *Mécanique des fluides* (Dunod, 1995)

[8] T.Farouk, B. Farouk, International Journal of Heat and Mass Transfer **50**, 4724 (2007)

[9] T.Farouk, B. Farouk, A. Gusol, International Journal of Heat and Mass Transfer **52**, 3320 (2009)

[10] H. Schlichting, *Boundary-Layer Theory* (Springer, 1979)

[11] J. Burazer, A. Cocic, M. Lecic, Thermal Science **20**, 1 (2016)

[12] J.J.V. Deemter, Applied Scientific Research, Section A pp. 174–196 (1952)